Evidence for amylose inclusion complexes with multiple acyl chain lipids using solid-state NMR and theoretical approaches

Adrien Schahl, Anne Lemassu, Franck Jolibois, Valérie Réat

Evidence for amylose inclusion complexes with multiple acyl chain lipids using solid-state NMR and theoretical approaches

Adrien Schahl[a],[b], Anne Lemassu[a], Franck Jolibois[b] and Valérie Réat*[a]

[a] A. Schahl, A. Lemassu, V. Réat
Institut de Pharmacologie et Biologie Structurale, IPBS,UMR5089, Université de Toulouse, CNRS, UPS,
BP 64182, 205 route de Narbonne, 31077 Toulouse, Cedex 04, France
E-mail: valerie.reat@ipbs.fr
[b] A. Schahl, F. Jolibois
LPCNO, Université Fédérale de Toulouse Midi-Pyrénées,UMR5215, INSA-CNRS-UPS
135 avenue de Rangueil, 31077 Cedex 4 Toulouse, France

Abstract: Amylose is known to form inclusion complexes in the presence of hydrophobic guests. Among lipids, only single-chain fatty acids have been reported as possible guests with the surrounding amylose in a well-defined V-helix conformation. Using experimental ^{13}C solid-state NMR, we studied the formation of inclusion complexes between amylose and a variety of multiple-chains lipids of increasing complexity. Molecular dynamics simulations and calculations of ^{13}C isotropic chemical shifts using the Density Functional Theory approach were performed to support the interpretation of experimental spectra. We provide unambiguous evidences that amylose forms inclusion complexes with lipids bearing multiple acyl chains. Amylose conformations around these lipids are characterized by {ϕ,ψ} anomeric bond dihedral angles near {115°,105°}. In the ^{13}C NMR spectra, this translates into C_1 and C_4 chemical shifts of 102.5 ppm and 81.1 ppm, regardless of the helical conformation of the amylose surrounding the acyl chains.

KEYWORDS: Starch • Lipids • solid-state NMR spectroscopy• Molecular dynamics simulation• Density functional calculation

1. Introduction

Starch, the major source of energy of numerous plants, is a mixture of two polysaccharides, amylose and amylopectin, composed largely of glucopyranose units, linked [α-1→4], although amylopectin contains up to 5% of residues linked [α-1→6]. Intensive research has been undertaken on these molecules in the pharmaceutical and food industries, due to their biodegradability, availability and ultrastructural properties. These two polysaccharides are known to form helical structures depending on their environment. In an aqueous environment, double helices termed A or B polymorphs are formed (Buléon et al., 2007; Poulhazan et al., 2018). However, in presence of a hydrophobic guest, these polysaccharides form helical inclusion complexes (Beeren & Hindsgaul, 2013; Obiro et al., 2012), in which the guest molecule is located within the hydrophobic cavity of the polysaccharide structure. When crystallized, these complexes are called V polymorphs. Amylose has been characterized as a stable host for small compounds, such as flavours (Nuessli et al., 2003; Tapanapunnitikul et al., 2008) and drugs (Carbinatto et al., 2016; Gao et al., 2017), but also for larger, extended molecules, such as fatty acids (Godet et al., 1993; Le et al., 2018; Lebail et al., 2000) and lysophospholipids (Eliasson, 1994; Wang et al., 2020).

It is generally thought that multiple-chain lipids are not able to form inclusion complexes with amylose. Indeed, studies performed on samples containing phospholipids or di-or tri-palmitate glycerol failed to detect the presence of helical amylose structures (Chao et al., 2018; Tang & Copeland, 2007). The solubility of the lipids during the complexation process is generally considered to be a limiting factor[20]. Recently, Sang et al. suggested that the palmitoyloleoylphosphatidylcholine (POPC) might be involved in the formation of inclusion complexes at low lipid/starch ratio (0.4% w/w) (Sang et al., 2019), using differential scanning calorimetry and X-ray diffraction. There is little other evidence for the existence of these multiple-chain lipid/amylose complexes and no experimental data regarding their structural characterization is available.

Among the experimental methods used to characterize such structures, solid-state NMR (ssNMR) has proven to be a powerful tool (Gidley & Bociek, 1988; Le-Bail et al., 2015; Le Bail et al., 2005; Lebail et al., 2000). The main advantage of ssNMR is that heterogeneous samples can be characterized and the presence of different structures revealed. In particular, the chemical shifts of the C_1 and C_4 carbons of the glycosidic unit (**Figure S1**) may be used as probes to characterize the structure of amylose (Lebail et al., 2000). These chemical shifts are sensitive to modification of the anomeric torsion angles (ϕ and ψ – see **Figure S1**) and/or the hydrogen bonding networks when the amylose conformation undergoes a transition from random coil, or A or B polymorphs to helical inclusion complexes (Schahl et al., 2021; Suzuki et al., 2009; Tafazzoli & Ghiasi, 2009).

Theoretical tools are also available to help characterize the three-dimensional structure of these complexes. Among them, numerous studies have been undertaken using all-atom molecular dynamics (MD). The behavior of folded amylose as well as the folding process itself has been characterized, in the presence and absence of guest molecules (Cheng et al., 2018, 2019; López et al., 2012;

Schahl et al., 2020; Tusch et al., 2011). In addition, the use of quantum mechanical methods is now suitable to study such systems in terms of their structural, electronic or spectroscopic properties. In particular, it has been shown that the dynamic properties of these complexes must be taken into account to accurately compute their NMR spectra (Schahl et al., 2020, 2021).

Here, we present an experimental ssNMR spectroscopy study, supported by MD simulations and quantum chemical computation of NMR parameters that provides experimental evidence for the formation of inclusion complexes of amylose with multiple-chains lipids and relates local structural features to experimental NMR signals of amylose. We first characterize the effect of unsaturation of the lipidic chains, through the study of samples containing palmitic and oleic acids. We show that inclusion complexes can be obtained in presence of the phosphatidylcholines, dipalmitoylphosphatidylcholine (DPPC), palmitoyloleoylphosphatidylcholine (POPC) and dioleoyl-phosphatidylcholine (DOPC), and that the amount of complex formed depends on the presence or absence of unsaturation in the acyl chains. We also examine the formation of inclusion complexes with phtiocerol dimycocerosate (PDIM), a lipid with an atypical structure extracted from *Mycobacterium tuberculosis* (*Mtb)* cell wall and identified as virulent factor (Forrellad et al., 2013).

2. Experimental Section

Materials: Amylose from potato, palmitic acid (PAL, C16:0), oleic acid (OLE, C18:1), 1,2-dipalmitoyl-sn-glycero-3-phosphocholine (DPPC, C16:0-C16:0), 1-palmitoyl-2-oleoyl-sn-glycero-3-phosphocholine (POPC, C16:0-C18:1) and 1,2-dioleoyl-sn-glycero-3-phosphocholine (DOPC, C18:1-C18:1) were purchased from Sigma Aldrich. The ratio of α(1 → 6) branches to α(1 → 4) main chain bonds in amylose was measured by liquid ^{1}H NMR, as described by (Tizzotti et al., 2011) and is <0.2%. Phtiocerol dimycocerosates (PDIM) were purified from cultures of *M. tuberculosis* H37Rv as described in (Lanéelle et al., 2021) (see also Supporting information).

Amylose/lipid complexation process and NMR sample preparation: For each sample, the amount of lipid added to amylose was calculated to give lipid/glucose ratio ranging from 1:8 to 1:128 lipid per glucose (mol/mol) and expressed in percent (L/G) (**Table S1**). For this purpose, the mass of amylose is converted, as a first approximation, into a number of moles of glucose ($M_{glucose}$ = 162 g.mol^{-1}). Complexes were prepared according to a published protocol (Lebail et al., 2000), using for each sample, 60 mg of potato amylose and the appropriate amount of lipid (**Table S1**) in 4 mL of solvent (see Supporting information for details). After washing steps, the resulting amylose/lipid precipitate was freeze-dried for 24 hours, weighted and stored at 4°C until. For NMR experiment, the lyophilized precipitate was hydrated with the same amount of water (50% w/w relative humidity). These samples may contain amylose/lipid inclusion complexes, lipid precipitates and/or amylose in double B-helix or unfold conformations, in proportions that may vary depending on the lipid.

NMR data acquisition: NMR experiments were performed using a Bruker DMX narrow bore spectrometer operating at a ^{1}H Larmor frequency of 500.13 MHz. Spectra were acquired using a 4 mm double-resonance H/X cross polarization magic angle spinning (CP-MAS) Bruker probe, at ωr/2π = 10 kHz sample spinning rate and at room temperature. ^{13}C chemical spectra were recorded using a standard one-dimensional CP-MAS sequence (see Supporting information for details). The ^{13}C spectra were referenced to TMS. CP build-up experiments recorded as function of CP contact time indicated that C_1 and C_4 carbons show similar behavior under CP conditions (see Supporting information), allowing the calculation of the fraction of amylose inclusion complex in NMR samples.

Determination of the inclusion complex amylose fraction in NMR samples: Eight Lorentzian functions were adjusted using DMFit software (Massiot et al., 2002) to fit the experimental ^{13}C NMR spectra in the range of glucose resonances (105 to 57 ppm). Three of these functions were used to reproduce the C_1 signals (one for amylose complexed with lipid at ~102 ppm and two for B-helix at ~100 and ~99 ppm), one for the C_4 signal of amylose complexed with lipid (~81 ppm), two for the C_6 signals (at ~59 and ~61 ppm) and the last two were adjusted to the two main features between 70 and 76 ppm (**Figure S3**). The percentage of amylose complexed with lipid in a NMR sample was defined as follows:

$$\%Amyplex = \left(\frac{Area_{C4C}}{Area_{C1T}} \times 100\right),$$

where $Area_{C4C}$ is the area under the Lorentzian function corresponding to the peak at 81 ppm, associated with the C_4 of the glucose residues in lipid/amylose complexes and $Area_{C1T}$ is the area under the three Lorentzian functions corresponding to the C_1 signals of all glucose residues in the sample (signals between 99 and 103 ppm). The error on %Amyplex is estimated at ±3%, considering the reproducibility of sample preparations and the precision of the Lorentzian adjustment.

Molecular dynamics simulations: A linear amylose chain of 45 α(1 → 4) bonded residues was built using the Leap program of the AMBER package. Initial Phi (ϕ = O5-C1-O4'-C4') and psi (ψ = C1-O4'-C4'-C3') dihedral angles of the anomeric bond were set to -93.4° and 93.8°, respectively, leading to an extended, unfolded conformation of the amylose. No α(1 → 6) branching linkages (present at only <0.2% in amylose used for experimental complexation, see materials paragraph) were added. Structures of PAL, OLE and PDIM were prepared using the Avogadro software while standard lipids such as DPPC, POPC and DOPC were prepared using the Leap program. The solvation parameters and MD procedure have been described previously (Schahl et al., 2020) (see Supporting information).

Structural analysis: The distribution of distances between the centers of mass of glucose residues [n] and [n+X] along the amylose chain (X = 6, 7 or 8) was determined to identify V_x-helical conformations. These distances were measured every 10 ps over the entire MD simulation (100ns). Density maps for the $\{\phi, \psi\}$ anomeric bond dihedral angles were calculated as described previously (Schahl et al., 2020, 2021) (see Supporting information), by extracting angles every 10 ps over the entire MD simulation.

Calculation of theoretical ^{13}C NMR spectra: 50 structures were extracted from the last 10 ns of each MD simulation. Using these structures, ^{13}C isotropic chemical shielding values were computed using the GIAO method (Ditchfield, 1972) at the B3LYP DFT level and using the 6-31G(d,p) basis set. For each carbon C_i, the chemical shielding was averaged over the set of 50 structures to obtain $<\sigma_i>$. Carbon atoms were separated into those belonging to glucose residues in helical amylose, and those in random coil amylose. In each category, chemical shielding values were averaged to obtain the set of chemical shielding values for the 6 carbons corresponding to one glucose residue. The theoretical NMR spectrum thus obtained is that of one "averaged" helical or random coil residue as described previously (Schahl et al., 2021) (see Supporting information for details).

3. Results and Discussion

3.1. **Fatty acid/amylose complexes: unsaturation in the acyl chains facilitates the formation of complex**.

The complexation of potato amylose with palmitic (PAL) or oleic (OLE) acids was performed using 5 initial lipid/glucose molar ratios (L/G, mol/mol). The ^{13}C NMR spectrum of each sample was recorded, and the amount of amylose in inclusion complex with lipids was determined (%Amyplex, see Experimental section for definition).
For both fatty acids, the ^{13}C NMR spectra of the precipitates resulting from lipid/amylose complexation show the characteristic features of inclusion complexes in a V-helix conformation (Gidley & Bociek, 1988; Lebail et al., 2000) (**Figure 1A and S4**).

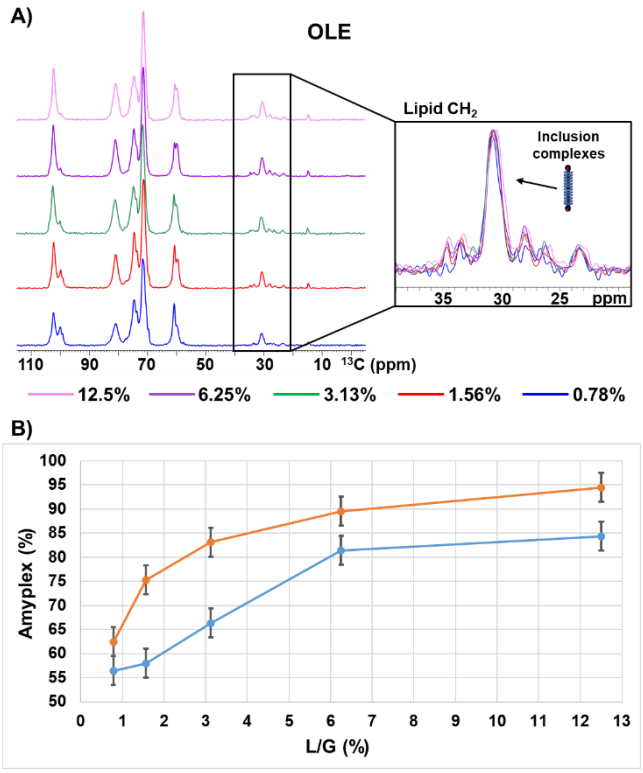

Figure 1. A) ^{13}C NMR spectra recorded on 50% (w/w) hydrated oleic acid (OLE) /amylose samples obtained with an initial lipid to glucose molar ratio of 0.78% (blue), 1.56% (red), 3.13% (green), 6.25% (purple) and 12.5% (pink). B) Percentage of amylose complexed with palmitic (blue) and oleic (orange) acids in NMR samples (%Amyplex) as a function of the initial L/G molar ratio.

The C_1, C_4 and C_6 carbons of the glucose unit (see **Figure S1** for carbon numbering) are assigned to peaks at 102.5, 81.1 and 59.8 ppm, respectively. The C_2, C_3 and C_5 carbons contribute to signal between 70 and 76 ppm. Our recent work suggests that the peak at 76 ppm also contains contributions of C_4 carbon of glucose units located between two successive V-helices (Schahl et al., 2020). Furthermore, signals between 98 and 101 ppm and at 60.5 ppm correspond to the C_1 and C_6 carbons of glucose units located in unstructured and/or B-polymorph fractions of amylose. The signals of the CH_2 groups composing the fatty acyl chain encapsulated in amylose are located at 30.7 ppm. For the sample with PAL obtained at the highest initial lipid concentration (**Figure S4**, L/G ratio = 12.5%), the signal of another population of CH_2 carbons is observed at 32.4 ppm, corresponding to lipid precipitate (Lebail et al., 2000). This signal is not found in samples containing OLE at any lipid concentration. For both lipids, an increase in L/G ratio is correlated to a decrease in signal intensity in the range 98-101 ppm and at 60.5 ppm. In parallel, the intensity of signals at 102.5 and 81.1 ppm (C_1 and C_4 carbons of glucose in amylose V-helix) increase with the lipid concentration (**Figure 1A. and S4**). This behavior has been reported previously for PAL/amylose complexes (Lebail et al., 2000) and was associated with an increase of amylose V-helix content. Increasing the L/G ratio also leads to a decrease of the C_6 signal at 60.8 ppm in favor of the signal at 59.8 ppm. This is consistent with our recent study (Schahl et al., 2020), in which we demonstrated that the signal at 59.8 ppm is due to C_6 carbons in V-helix structures. For both fatty acids, %Amyplex increases as a function of the L/G ratio (**Figure 1B**). It is higher in OLE samples suggesting that the addition of an unsaturation in the middle of a lipid chain promotes the formation of the amylose V-helices.

3.2. **Ability of lipids bearing multi-chains to form complexes with amylose.**

The ^{13}C NMR spectra of precipitates resulting from amylose complexations with DPPC, POPC and DOPC at several concentrations show a similar behavior to those recorded for samples containing fatty acids (**Figure 2A, S5 and S6)**. The chemical shifts of all carbons of the amylose are consistent with those associated with inclusion complexes in a V-helix conformation. However, some differences are observed for the CH_2 signal of the fatty acyl chains. The lipid precipitate signal is present at 32.4 ppm even at the lowest L/G ratio for DPPC samples (**Figure S5A**) and is shifted to 29.5 ppm for POPC and DOPC samples (**Figures 2A and S6**, L/G ratio of 6.25 and 12.5%). Differences are also observed in the values of %Amyplex calculated for each lipid and their evolution as a function of the L/G ratio (**Figure 2B, plain line**). For DPPC, %Amyplex increases from 55% to 70% for the first two values of the L/G ratio (0.78% and 1.56%) and then decreases to 55% for a L/G ratio of 3.13% (**Figure 2B, plain yellow line**). The formation of lipid precipitates, observable in the ^{13}C spectra even at the lowest L/G ratio (**Figure S5A, blue curve**), suggests that there may be a solubility issue for this lipid during the cooling step of the complexation protocol. To test this hypothesis, the protocol was adapted by doubling and quadrupling the complexation volume for samples with L/G ratios of 3.13% and 6.25%, respectively. The initial DPPC concentration being decreased, this should adversely affect the lipid precipitation process and increase the accessibility of DPPC for complexation with amylose. This was indeed confirmed by the observation of an increase in %Amyplex in the spectra obtained from these two "diluted" conditions (**Figure 2B, dashed yellow line**).At the highest L/G ratio tested, this value of 95% for %Amyplex is even higher than that obtained in the palmitic acid sample (%Amyplex(max) = 85%, **Figure 1B, blue curve**). It should be noted that a non-negligible amount of lipid precipitate

persists in these samples (**Figure S5B, purple and green curves**).

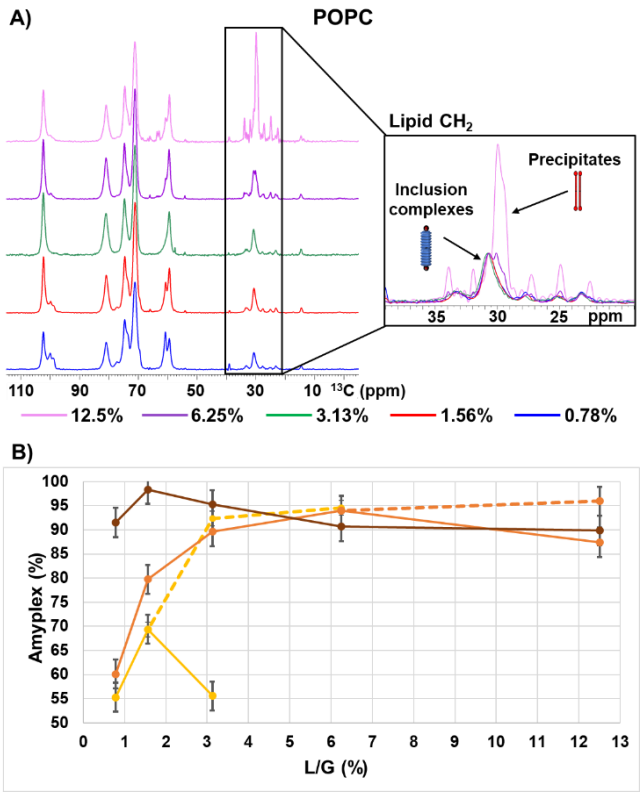

Figure 2 A) ^{13}C NMR spectra recorded on 50% (w/w) hydrated POPC/amylose samples obtained with an initial lipid to glucose molar ratio of 0.78% (blue), 1.56% (red), 3.13% (green), 6.25% (purple) and 12.5% (pink). B) Percentage of amylose complexed with DPPC (yellow), POPC (orange) and DOPC (brown) in NMR samples (%Amyplex) as a function of the initial L/G molar ratio. Yellow dashed line corresponds to DPPC samples for which the volume has been doubled (3.13%) or quadrupled (6.25%). Orange dashed line corresponds to POPC sample for which the volume has been quadrupled (12.5%).

For POPC, the %Amyplex curve shows an inflection similar to that observed for DPPC but only at the highest L/G ratio (**Figure 2B, plain orange line**). This final complexation experiment was again repeated using a quadrupled volume and again we observed an increase in %Amyplex for this "diluted" condition (**Figure2B, dashed orange line**). All samples prepared with DOPC contain more than 90% of amylose complexed with lipid, regardless of the L/G ratio used (**Figure 2B, brown line**) and high concentrations show lipid precipitates, characterized by the appearance of a peak at 29.5 ppm in ^{13}C NMR spectra.

Finally, the mycobacterial lipid PDIM also forms inclusion complexes with amylose, with an amount depending again on the initial L/G ratio (**Figure 3**). This type of lipid has a rather different structure from other lipids studied so far: it contains three longer hydrophobic chains (20 to 30 carbons), two of which carry four methyl groups adjacent to the ester functional groups (**Figure S2**), and no well-defined polar head. The two samples prepared at initial L/G ratios of 1.82% and 3.70% present the typical complexation signals for the C_1, C_4 and C_6 carbons and yield %Amyplex values of 41% and 77%. For the sample containing the lowest initial L/G ratio, there is clear indication of B-polymorph of amylose. The CH_2 signal at 30.7 ppm indicates the presence of encapsulated lipids only, suggesting that the structure of PDIM is less conducive to lipid/lipid interactions at low concentration compared to DPPC (**Figure S5A**).

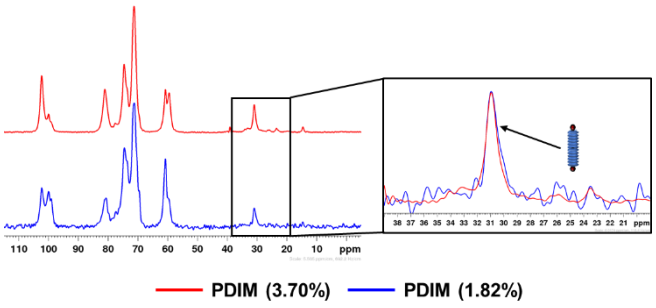

Figure 3. ^{13}C NMR spectra recorded on 50% (w/w) hydrated PDIM/amylose samples with an initial lipid to glucose molar ratio of 1.82% (blue) and 3.70% (red).

The behavior of samples containing fatty acids and phospholipids led us to postulate a competition mechanism between different states of the lipids and of the polysaccharides (**Figure 4**). At 90°C, the lipids and amylose are soluble in the mixture of DMSO/H_2O (3:5 v/v). The cooling process may lead to the precipitation of the two components in different forms. Lipids may precipitate, depending on their solubility, before the complexation with amylose takes place. The lipid/amylose complexes may be formed and precipitate. Amylose might also precipitate in B-double helix polymorphs if the initial concentration of lipids is too low. The competition between these different types of precipitation may be driven by the primary structure of the lipids. For fatty acids, the expected strength of lipid-lipid interactions can be correlated with the presence of an unsaturated bond that lowers the melting temperature from 63°C for PAL (C16:0 acyl chain) to 13°C for OLE (C18:1 acyl chain). This has the effect of decreasing the capacity of OLE to form lipid precipitates (**Figure 1A**) leaving OLE soluble and available for complexation with amylose, in the temperature range 90°C to 25°C. These results in a higher value of %Amyplex within the OLE/amylose samples compared to those obtained with PAL, regardless of the L/G ratio used (**Figure 1B**). Concerning complexation between phospholipids (DPPC, POPC and DOPC) and amylose, the addition of an acyl chain via the glycerol group of the phosphatidylcholines leads to an increase in inclusion complexes in the samples (**Figures 2B**), regardless of the L/G ratio used. For this, however, it is necessary to decrease the precipitation process for lipids containing saturated chains by lowering their initial concentration.

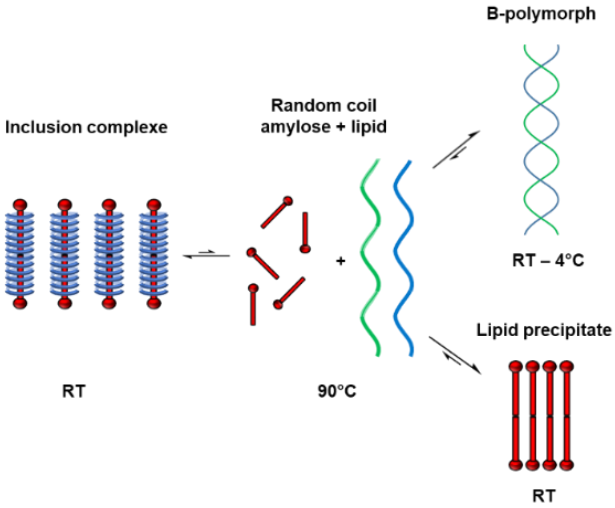

Figure 4. Schematic representation of the chemical equilibrium between the formation of inclusion complexes and the formation of lipid precipitates during the cooling of the mixture (See Experimental section)

For all lipids tested, the experimental NMR spectra of amylose are similar to the fatty acid one. To gain insight into the structuration of amylose around the lipids, we performed molecular modeling of amylose/lipid complexation to identify structural elements of amylose characteristic of the complexation and that could be at the origin of the NMR complexation signature.

3.3. Heterogeneity of the conformation of inclusion complexes.

Molecular dynamics simulations were performed to follow the complexation of one PAL, OLE, DPPC, POPC, DOPC or PDIM molecule with a 45 α(1 → 4) bonded residues amylose chain in an aqueous environment. While all lipids undergo encapsulation by amylose, the structures of the complexes obtained are different from one lipid to another, as illustrated in **Figure S7**. These snapshots represent single images from among the enormous diversity of possible amylose/lipid complex structures in solution and illustrate possible arrangements of amylose around lipid molecules. A stable and regular conformation of amylose in V_6-helix (V-helix conformation with 6-glucose units per helix-turn) is observed surrounding single-chain lipids (PAL and OLE), consistent with the results of previous MD simulations (Cheng et al., 2018, 2019; López et al., 2012; Schahl et al., 2020) and experimental data (Godet et al., 1993; Le et al., 2018). For DPPC, our simulation resulted in a conformation in which one fatty acyl chain is encapsulated in a stable V_6-helix of amylose. The release of one of the acyl chains from the helical structure of amylose has been discussed in a similar theoretical work (López et al., 2012). The DOPC and POPC MD simulations show that both tails can be encapsulated in amylose adopting a V-helix form. As a consequence, the diameter of the V-helix is enlarged locally, as more residues are needed to cover the lipid. The distribution of [n] – [n+X] distances (X=6, 7 or 8), calculated along the MD trajectories, indicates the formation of a mix of V_7- and V_8-helix (7 and 8-glucose units per helix-turn) around POPC and of V_6- and V_7 helix around the DOPC (Figure S8). This is associated with an increase of ~38% in the number of residues needed to cover the POPC and DOPC hydrophobic chains in comparison with fatty acids. These observations allow us to suppose that a similar behavior can be achieved by DPPC. In the absence of more extensive sampling of conformational space (which would require the use of more sophisticated MD methods such as replica exchange MD, beyond the scope of this study), we cannot exclude the possibility of a DPPC complex structure in which both acyl chains are encapsulated in amylose. A further MD study was performed to follow PDIM/amylose complexation and gain insight into a possible structural arrangement of amylose around this structurally very different lipid (**Figure S2**). In an aqueous environment, the lipid rapidly adopts (<2ns of simulation) a globular structure forming a cluster of hydrophobic chains. The amylose folds around this structure and, during the simulation, one of the acyl chains of PDIM is progressively extracted from the hydrophobic core to be surrounded, in an extended conformation, by the polysaccharide (**Figure S7**).

For all lipid/amylose MD simulation, glucose residues have been identified and separated between those in interaction with lipid molecule and the other in random-coil conformation, using their $\{\phi, \psi\}$ anomeric bond dihedral angles density map along the MD trajectories. For each simulation residues in a helical conformation give a density map with a maximum for $\{\phi, \psi\}$ angles around $\{115°, 105°\}$ (**Figure 5 and S9 – middle panels**) consistent with a previous study (Schahl et al., 2020). The remaining residues (in a random-coil conformation) all show a first local maximum for $\{\phi, \psi\}$ angles around $\{75°, 95°\}$ and a second of lower intensity around $\{100°, 110°\}$ (**Figure 5 and S9 – left panels**). These latter density maps are very similar to that obtained from the MD simulation of a single amylose chain in water (**Figure S9**). These observations reflect the random-coil to helix transition that the polysaccharide undergoes in water, which has also been characterized recently through MD simulations using different force fields (Koneru et al., 2019). Two ^{13}C NMR spectra of glucose units were then calculated (see experimental section), depending on their density map of $\{\phi, \psi\}$ angles. A theoretical spectrum for the glucose units in a helical conformation and that of the units in a random-coil conformation were obtained (**Figure 5 and S9, right panels, blue and red lines, respectively**). For each lipid/amylose complex, the averaged chemical shifts obtained for C_1 and C_4 are significantly higher in the spectrum of helical conformation (between 102-103 ppm and 80-82 ppm, respectively) than in the spectrum associated to random coil structure (between 100-101 ppm and 75-76 ppm, respectively). This analysis shows that the ^{13}C peaks of C_1 at 102.5 ppm and C_4 at 81.1 ppm observed experimentally can be associated to the maximum of $\{\phi, \psi\}$ angles density map calculated from the MD simulations at $\{115°, 105°\}$. They are both the signature of amylose glucose residues directly involved in lipid complexation, whatever their helical configuration.

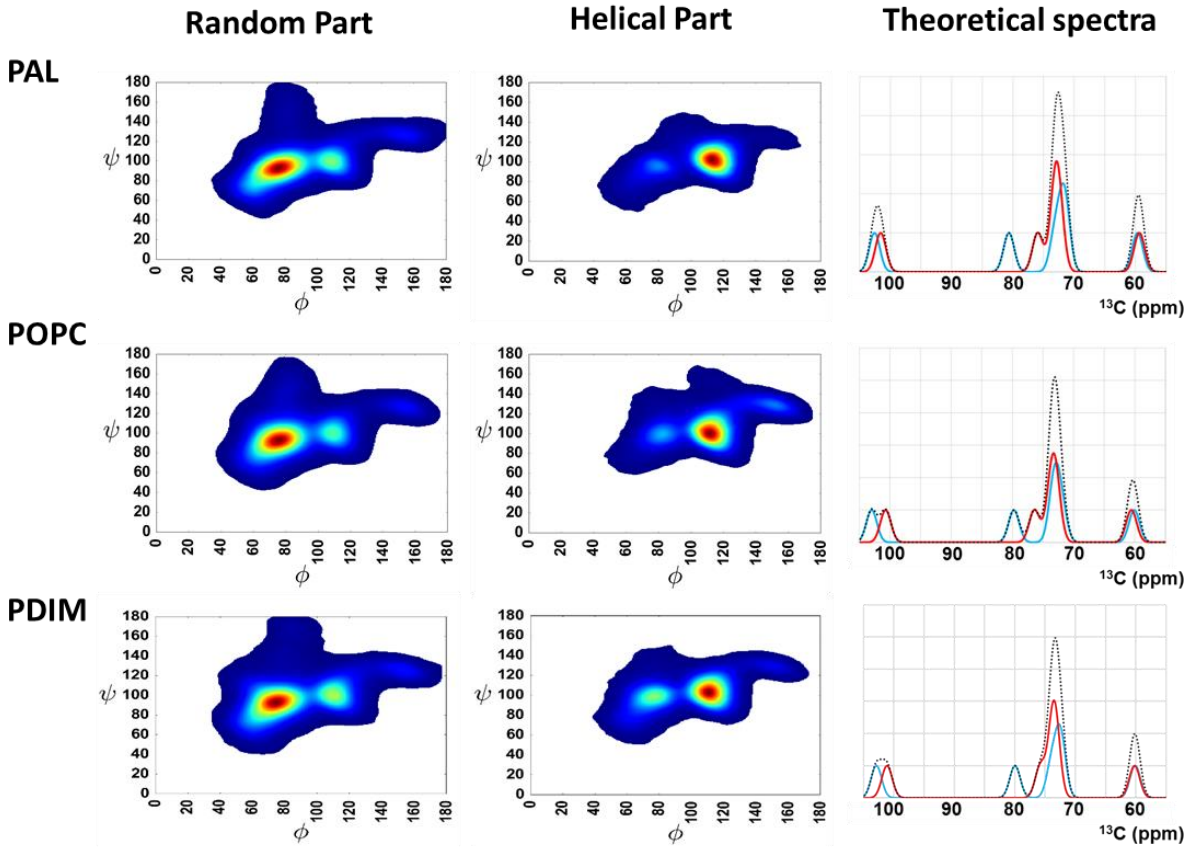

Figure 5. Density maps of $\{\phi,\psi\}$ anomeric bond dihedral angles (in degrees) over the entire MD simulation for PAL, POPC and PDIM/amylose systems taking into account only residues located in the random (left panel) or helical (middle panel) part of amylose.^{13}C NMR spectra (right panel) computed for structures extracted from MD of PAL, POPC or PDIM/amylose simulations, for residues in the helical (blue line) or random coil (red line) parts of the amylose or for all residues (black dotted line).

The inhomogeneity of the structures of inclusion complexes suggests that lipids containing multiple acyl chains are unlikely to induce ordered amylose structures when complexed, as already observed for fatty acids (Goderis et al., 2014; Le et al., 2018; Zabar et al., 2010). Rather, the helical structure of amylose would be inhomogeneous and randomly oriented with respect to each other in lipid/amylose precipitates, as proposed recently (Kong et al., 2019). This may explain why lipid/amylose complexes of the V-polymorph type could not be observed in the presence of glycerophospholipids using calorimetry or Xray crystallography experiments (Chao et al., 2018; Tang & Copeland, 2007). Experimentally, the NMR spectra show that all the multi-chain lipids can be encapsulated by amylose and a majority of the amylose is structured around the lipid (except for the lowest PDIM initial L/G ratio tested, **Figures 1B and 2B**).

Lipids containing only one hydrophobic chain are encapsulated by regular V_6-helical amylose in an extended conformation (see (Obiro et al., 2012) and references therein). The resulting regular V_6-helical amylose conformation shows density maps of $\{\phi,\psi\}$ dihedral angles with a single maximum located at {115°,105°} and is translated into C_1 and C_4 chemical shifts values of 102.5 and 81.1 ppm, respectively (Le et al., 2018; Lebail et al., 2000). As hydrophobic chains are added, the possible conformations adopted by the lipid and amylose inside the complexes become more diverse (**Figure 5**). Analysis of MD simulations of multi-chain lipid/amylose systems shows that two-chain lipids can be complexed by amylose with one or two encapsulated chains Furthermore, lipids may generate hydrophobic clusters of folded acyl chains which are more difficult to encapsulate in a regular V-helix conformation. However, analysis of the amylose conformations around these lipids shows density maps of $\{\phi,\psi\}$ dihedral angles with a maximum around $\{115°, 105°\}$, although no regular V_X-helix conformation is always recognizable in the amylose structure. These $\{\phi,\psi\}$ dihedral angle values define this anomeric bond conformation as a signature of the structural arrangement of the amylose around acyl chains and correspond to chemical shift values for C_1 and C_4 carbons close to 102.5 and 81.1 ppm, respectively.

4. Conclusions

Combining experimental ssNMR spectra, molecular dynamics simulation and quantum chemical computation of NMR parameters we provide evidence for the formation of inclusion complexes of amylose with lipids bearing multiple acyl chains. We show that inclusion complexes can be obtained in the presence of phosphatidylcholines and that the amount of complex formed depends on the presence of unsaturated groups in the acyl chains. Amylose

conformations around the lipids are characterized by $\{\phi, \psi\}$ anomeric bond dihedral angles near $\{115°, 105°\}$. In the experimental ^{13}C NMR spectra, this translates into C_1 and C_4 chemical shifts values of 102.5 and 81.1 ppm, respectively. To the best of our knowledge, inclusion complexes of amylose have rarely been characterized experimentally in the presence of multiple-chain lipids. This may be explained by the high homogeneity needed for characterization of these complexes, by methods such as differential scanning calorimetry, rapid visco analyser, or even crystallography. Solid-state NMR spectroscopy is sensitive to local conformation and no dependent on long-range order or high homogeneity. It appears as an efficient tool for revealing these inclusion complexes. It should be noted that amylose constitutes the simplest model of polysaccharides. Consequently, this study represents a first step towards the analysis of complexation process of multiple chains lipids with more complex polysaccharides, branched or not branched, such as amylopectin, cellulose, α-glucan or glycogen.

Acknowledgements

A.S. was a recipient of a PhD scholarship from University of Toulouse and the “Région Occitanie”. This work was supported by a CNRS-MITI grant “Modélisation du vivant” 2019 and 2020. This work was granted access to the HPC resources of CALMIP supercomputing center under the allocation 2018-p0758 and of CINES and IDRIS supercomputing center under the allocation 2019-A0060810816 made by GENCI. We thank the Integrated Screening Platform of Toulouse (PICT, IBiSA) for providing access to NMR equipment funded by CNRS, Université de Toulouse–Université Paul Sabatier, European Structural Funds (Fonds Européens de Développement Régional) and Région Occitanie. The authors thank Alain Milon for fruitful discussions of the results and Andrew Atkinson for meticulous correction of the manuscript.

References

Beeren, S. R., & Hindsgaul, O. (2013). Nature’s dendrimer: Characterizing amylopectin as a multivalent host. *Angewandte Chemie - International Edition*, *52*(43), 11265–11268. https://doi.org/10.1002/anie.201305132

Buléon, A., Véronèse, G., & Putaux, J. L. (2007). Self-association and crystallization of amylose. *Australian Journal of Chemistry*, *60*(10), 706–718. https://doi.org/10.1071/CH07168

Carbinatto, F. M., Ribeiro, T. S., Colnago, L. A., Evangelista, R. C., & Cury, B. S. F. (2016). Preparation and Characterization of Amylose Inclusion Complexes for Drug Delivery Applications. *Journal of Pharmaceutical Sciences*, *105*(1), 231–241. https://doi.org/10.1002/jps.24702

Chao, C., Yu, J., Wang, S., Copeland, L., & Wang, S. (2018). Mechanisms Underlying the Formation of Complexes between Maize Starch and Lipids. *Journal of Agricultural and Food Chemistry*, *66*(1), 272–278. https://doi.org/10.1021/acs.jafc.7b05025

Cheng, L., Feng, T., Zhang, B., Zhu, X., Hamaker, B., Zhang, H., & Campanella, O. (2018). A molecular dynamics simulation study on the conformational stability of amylose-linoleic acid complex in water. *Carbohydrate Polymers*, *196*, 56–65. https://doi.org/10.1016/j.carbpol.2018.04.102

Cheng, L., Zhu, X., Hamaker, B. R., Zhang, H., & Campanella, O. H. (2019). Complexation process of amylose under different concentrations of linoleic acid using molecular dynamics simulation. *Carbohydrate Polymers*. https://doi.org/10.1016/j.carbpol.2019.04.013

Ditchfield, R. (1972). Molecular Orbital Theory of Magnetic Shielding and Magnetic Susceptibility. *The Journal of Chemical Physics*. https://doi.org/10.1063/1.1677088

Eliasson, A. C. (1994). Interactions between starch and lipids studied by DSC. *Thermochimica Acta*, *246*(2), 343–356. https://doi.org/10.1016/0040-6031(94)80101-0

Forrellad, M. A., Klepp, L. I., Gioffré, A., Sabio y García, J., Morbidoni, H. R., de la Paz Santangelo, M., Cataldi, A. A., & Bigi, F. (2013). Virulence factors of the Mycobacterium tuberculosis complex. *Virulence*, *4*(1), 3–66. https://doi.org/10.4161/viru.22329

Gao, W., Liu, Y., Jing, G., Li, K., Zhao, Y., Sha, B., Wang, Q., & Wu, D. (2017). Rapid and efficient crossing blood-brain barrier: Hydrophobic drug delivery system based on propionylated amylose helix nanoclusters. *Biomaterials*, *113*, 133–144. https://doi.org/10.1016/j.biomaterials.2016.10.045

Gidley, M. J., & Bociek, S. M. (1988). 13C CP/MAS NMR Studies of Amylose Inclusion Complexes, Cyclodextrins, and the Amorphous Phase of Starch Granules: Relationships Between Glycosidic Linkage Conformation and Solid-State 13C Chemical Shifts. *Journal of the American Chemical Society*, *110*(12), 3820–3829. https://doi.org/10.1021/ja00220a016

Goderis, B., Putseys, J. A., Gommes, C. J., Bosmans, G. M., & Delcour, J. A. (2014). The structure and thermal stability of amylose-lipid complexes: A case study on amylose-glycerol monostearate. *Crystal Growth and Design*, *14*(7), 3221–3233. https://doi.org/10.1021/cg4016355

Godet, M. C., Buléon, A., Tran, V., & Colonna, P. (1993). Structural features of fatty acid-amylose complexes. *Carbohydrate Polymers*, *21*(2–3), 91–95. https://doi.org/10.1016/0144-8617(93)90003-M

Koneru, J. K., Zhu, X., & Mondal, J. (2019). A Quantitative Assessment of the Conformational Heterogeneity in Amylose across Force Fields. *Journal of Chemical Theory and Computation*. https://doi.org/10.1021/acs.jctc.9b00630

Kong, L., Perez-Santos, D. M., & Ziegler, G. R. (2019). Effect of guest structure on amylose-guest inclusion complexation. *Food Hydrocolloids*, *97*(June), 105188. https://doi.org/10.1016/j.foodhyd.2019.105188

Lanéelle, M.-A., Spina, L., Nigou, J., Lemassu, A., & Daffé, M. (2021). Lipid and Lipoarabinomannan Isolation and Characterization. In *Mycobacteria Protocols* (Issue Chapter 4, pp. 109–150). https://doi.org/10.1007/978-1-0716-1460-0_4

Le-Bail, P., Lorentz, C., Pencreac’h, G., Soultani-Vigneron, S., Pontoire, B., Giraldo, L. J. L., Villeneuve, P., Hendrickx, J., & Tran, V. (2015). Trapping by amylose of the aliphatic chain grafted onto chlorogenic acid: Importance of the graft position. *Carbohydrate Polymers*, *117*, 910–916. https://doi.org/10.1016/j.carbpol.2014.10.029

Le Bail, P., Rondeau, C., & Buléon, A. (2005). Structural investigation of amylose complexes with small ligands: Helical conformation, crystalline structure and thermostability. *International Journal of Biological Macromolecules*, *35*(1–2), 1–7. https://doi.org/10.1016/j.ijbiomac.2004.09.001

Le, C.-A.-K., Choisnard, L., Wouessidjewe, D., & Putaux, J.-L. (2018). Polymorphism of crystalline complexes of V-amylose with fatty acids. *International Journal of Biological Macromolecules*, *119*, 555–564. https://doi.org/10.1016/j.ijbiomac.2018.07.163

Lebail, P., Buleon, A., Shiftan, D., & Marchessault, R. H. (2000). Mobility of lipid in complexes of amylose-fatty acids by deuterium and 13C solid state NMR. *Carbohydrate Polymers*, *43*(4), 317–326. https://doi.org/10.1016/S0144-8617(00)00180-6

López, C. A., de Vries, A. H., & Marrink, S. J. (2012). Amylose folding under the influence of lipids. *Carbohydrate Research*, *364*, 1–7. https://doi.org/10.1016/j.carres.2012.10.007

Massiot, D., Fayon, F., Capron, M., King, I., Le Calvé, S., Alonso, B., Durand, J.-O., Bujoli, B., Gan, Z., & Hoatson, G. (2002). Modelling one- and two-dimensional solid-state NMR spectra. *Magnetic Resonance in Chemistry*, *40*(1), 70–76. https://doi.org/10.1002/mrc.984

Nuessli, J., Putaux, J. L., Le Bail, P., & Buléon, A. (2003). Crystal structure of amylose complexes with small ligands. *International Journal of Biological Macromolecules*, *33*(4–5), 227–234. https://doi.org/10.1016/j.ijbiomac.2003.08.009

Obiro, W. C., Sinha Ray, S., & Emmambux, M. N. (2012). V-amylose Structural Characteristics, Methods of Preparation, Significance, and Potential Applications. *Food Reviews International*, *28*(4), 412–438. https://doi.org/10.1080/87559129.2012.660718

Poulhazan, A., Arnold, A. A., Warschawski, D. E., & Marcotte, I. (2018). Unambiguous ex situ and in cell 2D 13 C solid-state nmr characterization of starch and its constituents. *International Journal of Molecular Sciences*, *19*(12). https://doi.org/10.3390/ijms19123817

Sang, S., Chen, Y., Zhu, X., Narsimhan, G., Hu, Q., Jin, Z., & Xu, X. (2019). Effect of egg yolk lipids on structure and properties of wheat starch in steamed bread. *Journal of Cereal Science*, *86*(October 2018), 77–85. https://doi.org/10.1016/j.jcs.2019.01.009

Schahl, A., Gerber, I. C., Réat, V., & Jolibois, F. (2021). Diversity of the Hydrogen Bond Network and Its Impact on NMR Parameters of Amylose B Polymorph: A Study Using Molecular Dynamics and DFT Calculations Within Periodic Boundary Conditions. *The Journal of Physical Chemistry B*, *125*(1), 158–168. https://doi.org/10.1021/acs.jpcb.0c08631

Schahl, A., Réat, V., & Jolibois, F. (2020). Structures and NMR spectra of short amylose-lipid complexes. Insight using molecular dynamics and DFT quantum chemical calculations. *Carbohydrate Polymers*, *235*(January), 115846. https://doi.org/10.1016/j.carbpol.2020.115846

Suzuki, S., Horii, F., & Kurosu, H. (2009). Theoretical investigations of 13C chemical shifts in glucose, cellobiose, and native cellulose by quantum chemistry calculations. *Journal of Molecular Structure*, *921*(1–3), 219–226. https://doi.org/10.1016/j.molstruc.2009.01.002

Tafazzoli, M., & Ghiasi, M. (2009). Structure and conformation of α-, β- and γ-cyclodextrin in solution: Theoretical approaches and experimental validation. *Carbohydrate Polymers*, *78*(1), 10–15. https://doi.org/10.1016/j.carbpol.2009.02.020

Tang, M. C., & Copeland, L. (2007). Analysis of complexes between lipids and wheat starch. *Carbohydrate Polymers*, *67*(1), 80–85. https://doi.org/10.1016/j.carbpol.2006.04.016

Tapanapunnitikul, O., Chaiseri, S., Peterson, D. G., & Thompson, D. B. (2008). Water solubility of flavor compounds influences formation of flavor inclusion complexes from dispersed high-amylose maize starch. *Journal of Agricultural and Food Chemistry*, *56*(1), 220–226. https://doi.org/10.1021/jf071619o

Tizzotti, M. J., Sweedman, M. C., Tang, D., Schaefer, C., & Gilbert, R. G. (2011). New 1H NMR procedure for the characterization of native and modified food-grade starches. *Journal of Agricultural and Food Chemistry*, *59*(13), 6913–6919. https://doi.org/10.1021/jf201209z

Tusch, M., Krüger, J., & Fels, G. (2011). Structural stability of V-amylose helices in water-DMSO mixtures analyzed by molecular dynamics. *Journal of Chemical Theory and Computation*, *7*(9), 2919–2928. https://doi.org/10.1021/ct2005159

Wang, S., Chao, C., Cai, J., Niu, B., Copeland, L., & Wang, S. (2020). Starch–lipid and starch–lipid–protein complexes: A comprehensive review. *Comprehensive Reviews in Food Science and Food Safety*, *19*(3), 1056–1079. https://doi.org/10.1111/1541-4337.12550

Zabar, S., Lesmes, U., Katz, I., Shimoni, E., & Bianco-Peled, H. (2010). Structural characterization of amylose-long chain fatty acid complexes produced via the acidification method. *Food Hydrocolloids*, *24*(4), 347–357. https://doi.org/10.1016/j.foodhyd.2009.10.015